Supporting Information

Towards an ab initio description of optical spectra of light-harvesting antennae: Application to the CP29 complex of photosystem II

Sandro Jurinovich[a], Lucas Viani[a], Ingrid G. Prandi[a], Thomas Renger[b], Benedetta Mennucci[a]

[a]Dipartimento di Chimica e Chimica Industriale,
University of Pisa, Via G. Moruzzi 3, I-56124 Pisa, Italy

[b]Institut für Theoretische Physik
Johannes Kepler Universität Linz, Altenberger Str. 69, 4040 Linz, Austria

This supporting information is divided in three sections. Section 1 is dedicated to tables, section 2 to figures and section 3 describes in details the analysis of the impact of the neighboring residues in the site energy shift of pigments a604 and b608 when using the crystal structure.
The figures and tables are grouped by subject, namely:

Tables S1-S2: Site energies
Table S3: Structural properties of the complex
Tables S4-S5 Excitonic matrices derived for the crystalline and MD approaches

Figures S1: Transition dipole and Linear Dichroism spectra
Figures S2-S14: Time evolution of the site energies of the different pigments along the MD trajectory
Figures S15: Simulated broadenings and Linear Dichroism spectra
Figure S16: Contribution of the different pigments to the excitonic states along the MD trajectory.

1. Tables

	Chl *a*		Chl *b*		ΔE
	E	μ^2	E	μ^2	
Exp.[a]	1.916	21.0	1.987	14.7	0.071
VAC@MD	2.025	28.0	2.079	20.5	0.054
Exp.[b]	1.824	27.0	1.905	19.0	0.081
MMPol@MD	1.972	40.4	2.045	25.1	0.073

Table S1. Average site energies (eV) and square of the electric transition dipole moments (D^2) of Chl *a* and *b* calculated at TDCAM-B3LYP/6-31G(d) level in *vacuo* and with the MMPol environment description. [a]Experimental values for site energies and electric transition dipole moments in *vacuo* are estimated from Ref. 1 and Ref. 2 respectively. [b]Experimental values for site energies and electric transition dipole moments estimated in protein-like environment are taken from Ref. 3.

	VAC@MD		MMPol@MD	
	<ε>	σ	<ε>	σ
a602	2.032	0.060	1.971	0.069
a603	2.026	0.058	1.974	0.065
a604	2.026	0.056	1.968	0.063
a609	2.022	0.060	1.958	0.068
a610	2.020	0.057	1.975	0.063
a611	2.022	0.056	1.976	0.066
a612	2.031	0.058	1.975	0.068
a613	2.029	0.054	1.971	0.060
a615	2.026	0.058	1.987	0.069
b606	2.067	0.059	2.043	0.065
b607	2.075	0.058	2.036	0.062
b608	2.080	0.063	2.039	0.070
b614	2.081	0.059	2.046	0.061
	<σ>	0.058	<σ>	0.065

Table S2. Average pigment site energies <ε> (eV) and relative standard deviations σ (eV) along the MD trajectory computed in *vacuo* and with MMPol environmental description. The average standard deviation <σ> standard deviation is also shown.

	a602	a603	a604	b606	b607	b608	a609	a610	a611	a612	a613	b614	a615
a602	-	12.0	25.5	27.5	25.5	21.9	18.3	16.5	16.8	18.3	19.7	25.6	13.2
a603	12.3	-	19.5	18.7	15.2	18.2	9.4	19.0	25.5	23.1	20.2	28.6	24.1
a604	26.1	20.1	-	8.3	12.2	18.6	18.0	18.6	27.3	19.4	21.3	26.5	30.5
b606	28.1	19.1	7.9	-	9.9	16.1	14.1	21.2	33.1	25.7	27.0	33.5	35.2
b607	26.3	16.5	12.3	10.3	-	22.4	15.3	25.4	33.1	27.4	21.8	29.7	34.4
b608	22.5	18.7	18.6	17.4	24.4	-	10.9	12.0	28.9	23.0	31.9	37.9	29.4
a609	18.2	8.8	18.4	15.1	17.2	12.2	-	17.5	30.0	25.5	27.3	35.1	29.4
a610	17.3	19.6	18.9	22.2	26.6	11.7	18.1	-	17.5	12.1	25.6	29.5	19.1
a611	16.6	26.1	28.6	34.2	33.8	28.8	30.2	17.7	-	9.1	19.3	18.6	6.7
a612	18.6	24.0	20.7	27.0	28.2	23.4	26.3	12.5	9.2	-	18.5	19.2	14.3
a613	21.3	23.1	23.2	28.5	22.8	33.8	29.4	27.0	20.0	18.8	-	9.2	20.9
b614	26.7	31.2	29.2	35.7	31.2	39.4	37.2	30.6	19.1	19.5	9.3	-	21.8
a615	11.8	23.2	31.1	35.4	34.0	29.3	28.5	19.7	7.4	14.8	20.9	21.9	-

Table S3. Inter-pigment distance matrix based on crystal structure (upper triangle) and averaged over MD trajectory (lower triangle). Distances (in Å) have been computed using the geometrical center determined by the heavy atoms of the Chl ring.

	a602	a603	a604	b606	b607	b608	a609	a610	a611	a612	a613	b614	a615
a602	15987	17.6	-7.9	-5.6	-6.9	-7.4	-31.2	12.6	-3.2	-16.4	-3.0	0.1	-58.4
a603	17.6	15922	1.0	5.4	-9.9	6.5	128.0	-14.4	0.6	-1.0	3.2	5.5	3.0
a604	-7.9	1.0	15579	104.5	35.2	4.8	2.5	-2.3	5.3	2.3	-5.0	-3.7	-6.1
b606	-5.6	5.4	104.5	16897	24.4	3.5	-12.1	-2.4	2.6	0.9	-2.0	-1.7	-3.4
b607	-6.9	-9.9	35.2	24.4	16630	4.6	8.5	0.1	2.8	1.9	-4.2	-2.0	-3.8
b608	-7.4	6.5	4.8	3.5	4.6	16159	47.8	-49.6	6.9	-0.4	-3.8	-1.5	-8.3
a609	-31.2	128.0	2.5	-12.1	8.5	47.8	16092	8.3	4.8	-0.5	-5.1	-2.9	-9.9
a610	12.6	-14.4	-2.3	-2.4	0.1	-49.6	8.3	16149	36.5	9.9	-8.2	-0.6	-12.4
a611	-3.2	0.6	5.3	2.6	2.8	6.9	4.8	36.5	15950	-102.2	-0.9	-2.0	-147.3
a612	-16.4	-1.0	2.3	0.9	1.9	-0.4	-0.5	9.9	-102.2	16172	-1.8	-0.2	-8.2
a613	-3.0	3.2	-5.0	-2.0	-4.2	-3.8	-5.1	-8.2	-0.9	-1.8	16006	13.3	4.1
b614	0.1	5.5	-3.7	-1.7	-2.0	-1.5	-2.9	-0.6	-2.0	-0.2	13.3	16675	2.0
a615	-58.4	3.0	-6.1	-3.4	-3.8	-8.3	-9.9	-12.4	-147.3	-8.2	4.1	2.0	15896

Table S4. Excitonic matrix from MMPol@CRY calculations (all values are in cm^{-1}). Couplings are scaled by a factor 0.73 as described in the paper.

	a602	a603	a604	b606	b607	b608	a609	a610	a611	a612	a613	b614	a615
a602	15900	44.6	7.5	6.0	6.1	-5.4	-30.0	-11.9	-6.5	15.8	-1.4	1.7	64.4
a603	44.6	15923	-3.6	-6.1	8.1	3.1	130.8	12.8	-0.5	-1.6	4.0	-3.8	-2.6
a604	7.5	-3.6	15874	86.1	26.8	-7.0	-6.1	-3.1	-3.3	2.3	4.0	-2.9	-4.7
b606	6.0	-6.1	86.1	16481	20.7	-7.1	-1.8	-1.6	-2.6	2.5	2.9	-1.2	-3.2
b607	6.1	8.1	26.8	20.7	16421	-4.4	-11.2	1.0	-2.6	2.5	4.4	-1.8	-3.0
b608	-5.4	3.1	-7.0	-7.1	-4.4	16444	31.7	63.3	5.5	-2.7	-3.4	0.9	6.6
a609	-30.0	130.8	-6.1	-1.8	-11.2	31.7	15788	-5.5	4.5	-1.5	-4.9	1.9	8.1
a610	-11.9	12.8	-3.1	-1.6	1.0	63.3	-5.5	15926	-31.1	36.5	7.2	-0.1	-7.8
a611	-6.5	-0.5	-3.3	-2.6	-2.6	5.5	4.5	-31.1	15934	135.6	-8.1	-3.4	105.1
a612	15.8	-1.6	2.3	2.5	2.5	-2.7	-1.5	36.5	135.6	15928	3.1	2.5	-5.8
a613	-1.4	4.0	4.0	2.9	4.4	-3.4	-4.9	7.2	-8.1	3.1	15900	12.2	-4.2
b614	1.7	-3.8	-2.9	-1.2	-1.8	0.9	1.9	-0.1	-3.4	2.5	12.2	16501	-3.9
a615	64.4	-2.6	-4.7	-3.2	-3.0	6.6	8.1	-7.8	105.1	-5.8	-4.2	-3.9	16027

Table S5. Excitonic matrix from MMPol@MD calculations (all values are in cm^{-1}). Couplings are scaled by a factor 0.73 as described in the paper.

2. Figures

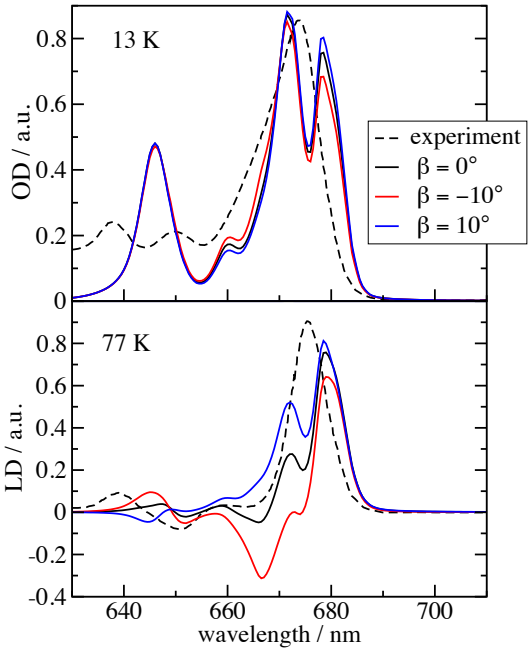

Figure S1. Effect of the Q_y dipole orientation on the low temperature absorbance and linear dichroism spectra comparing three different cases: electric transition dipole moment align along the NB-ND axis (β=0°) and rotated of β +/- 10° with respect to this.

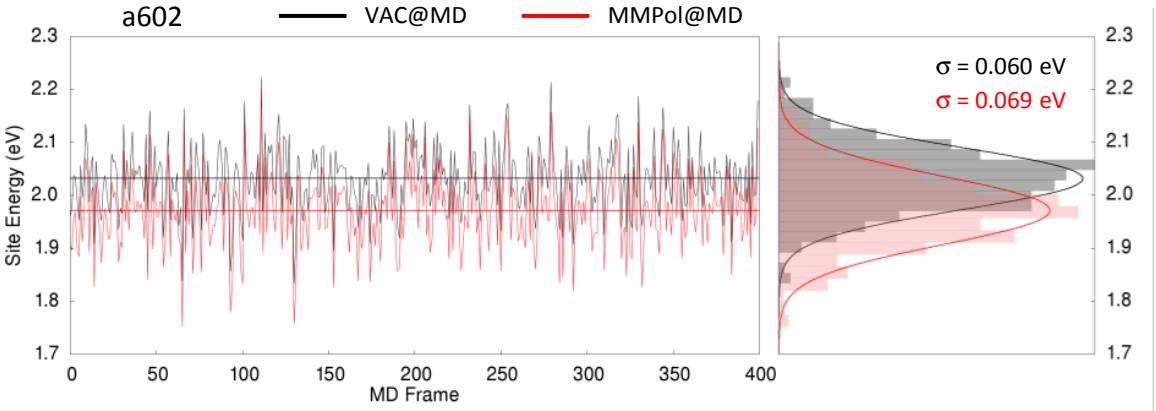

Figure S2. Site energies and relative distributions of pigment a602 along the MD trajectory computed in vacuum (black color) and with the MMPol description (red line).

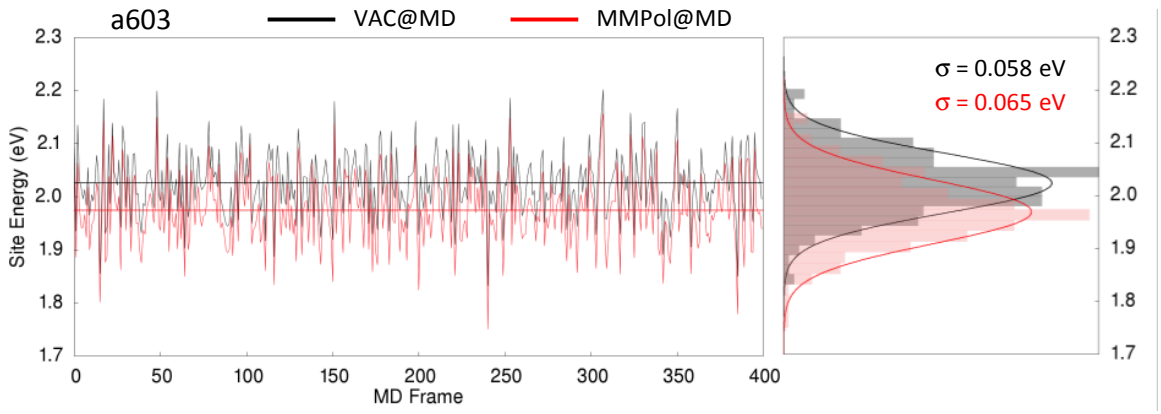

Figure S3. Site energies and relative distributions of pigment a603 along the MD trajectory computed in vacuum (black color) and with the MMPol description (red line).

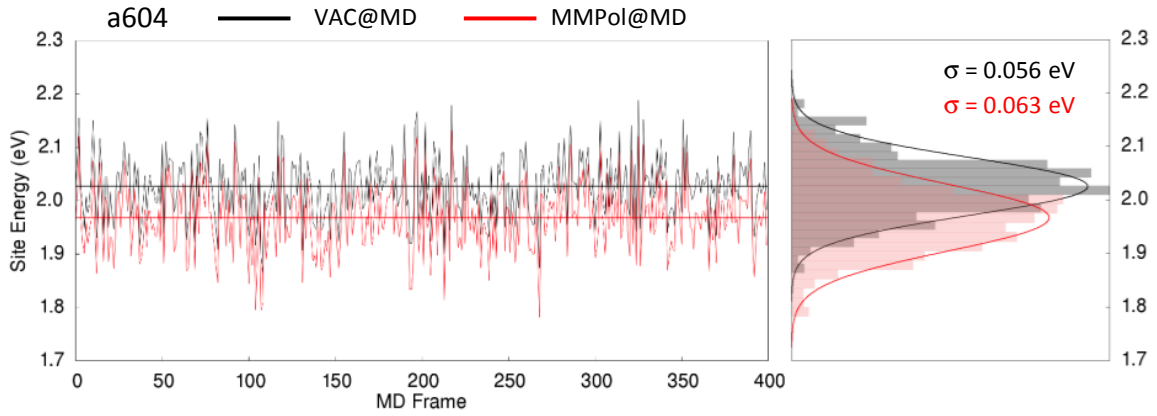

Figure S4. Site energies and relative distributions of pigment a604 along the MD trajectory computed in vacuum (black color) and with the MMPol description (red line).

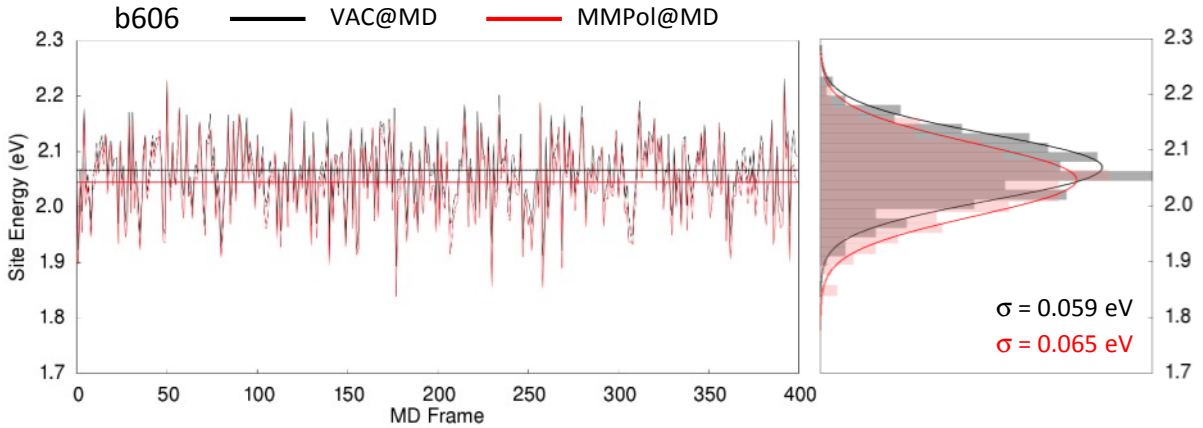

Figure S5. Site energies and relative distributions of pigment b606 along the MD trajectory computed in vacuum (black color) and with the MMPol description (red line).

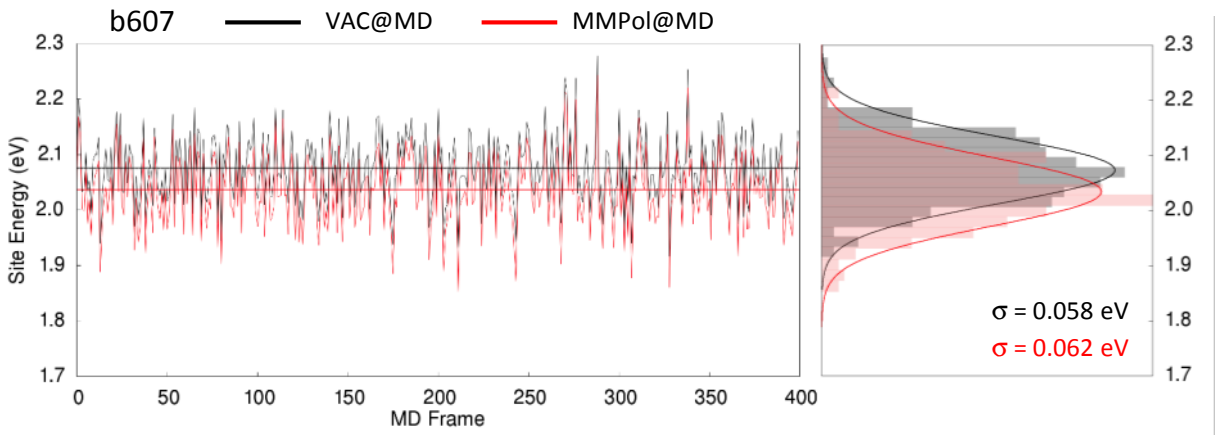

Figure S6. Site energies and relative distributions of pigment b607 along the MD trajectory computed in vacuum (black color) and with the MMPol description (red line).

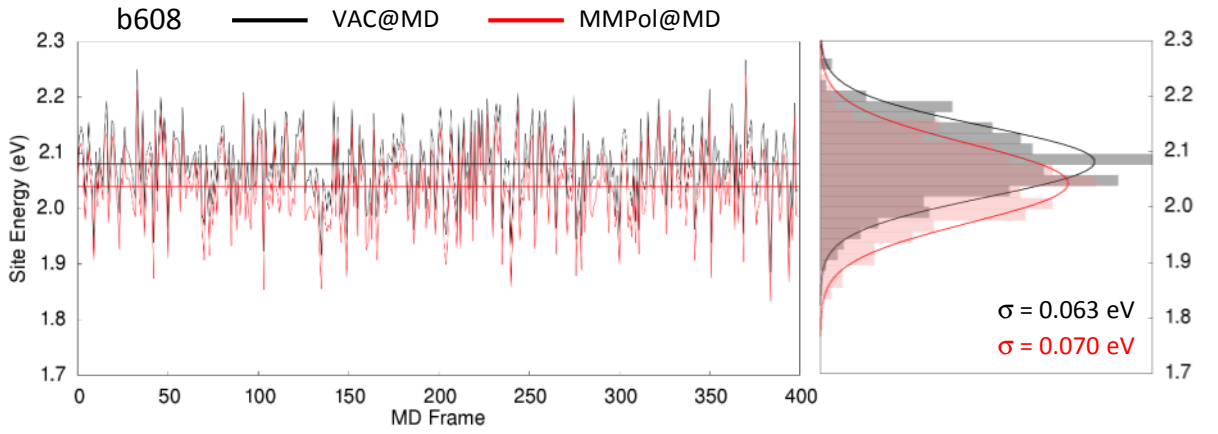

Figure S7. Site energies and relative distributions of pigment b608 along the MD trajectory computed in vacuum (black color) and with the MMPol description (red line).

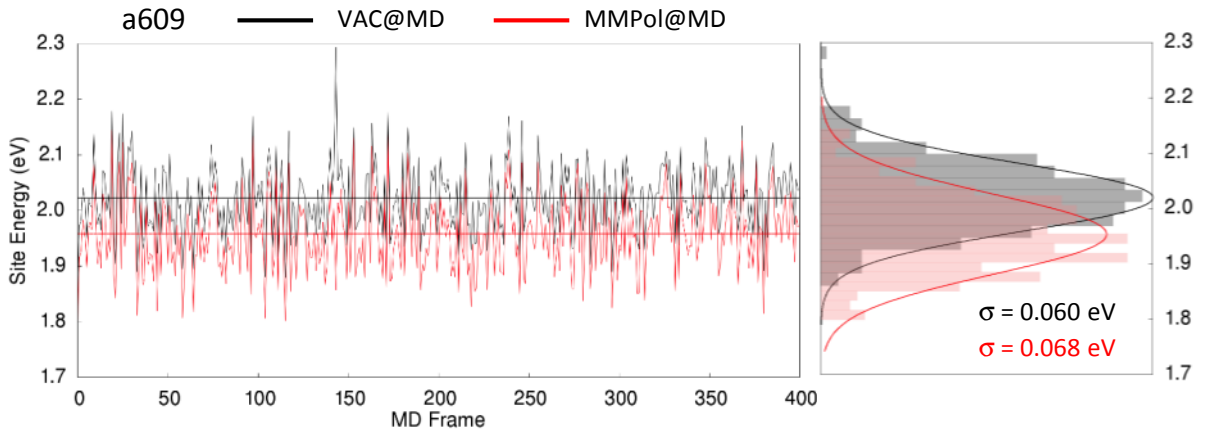

Figure S8. Site energies and relative distributions of pigment a609 along the MD trajectory computed in vacuum (black color) and with the MMPol description (red line).

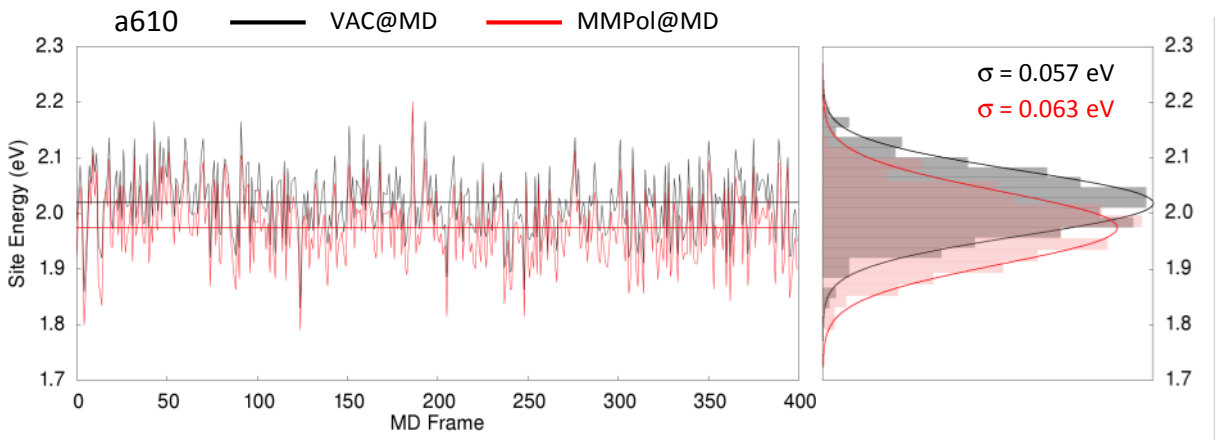

Figure S9. Site energies and relative distributions of pigment a610 along the MD trajectory computed in vacuum (black color) and with the MMPol description (red line).

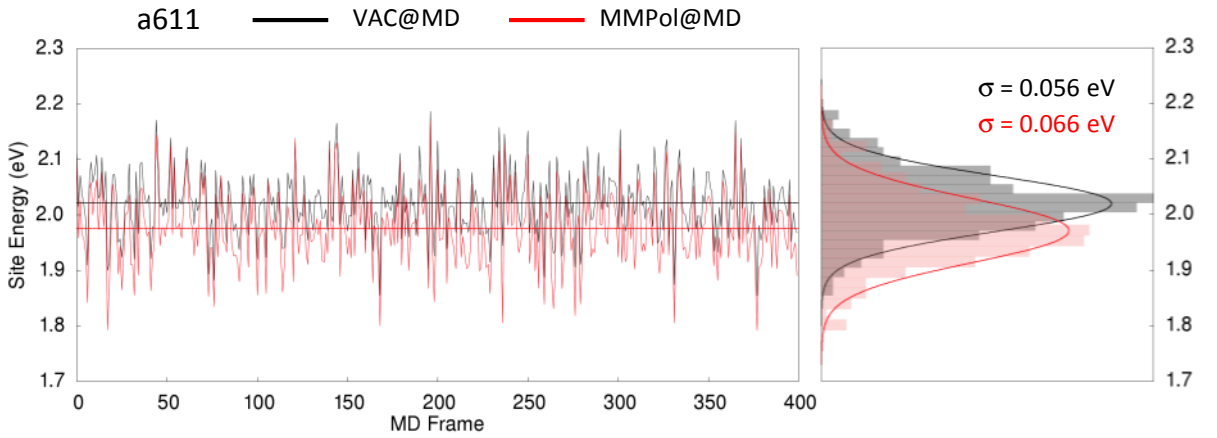

Figure S10. Site energies and relative distributions of pigment a611 along the MD trajectory computed in vacuum (black color) and with the MMPol description (red line).

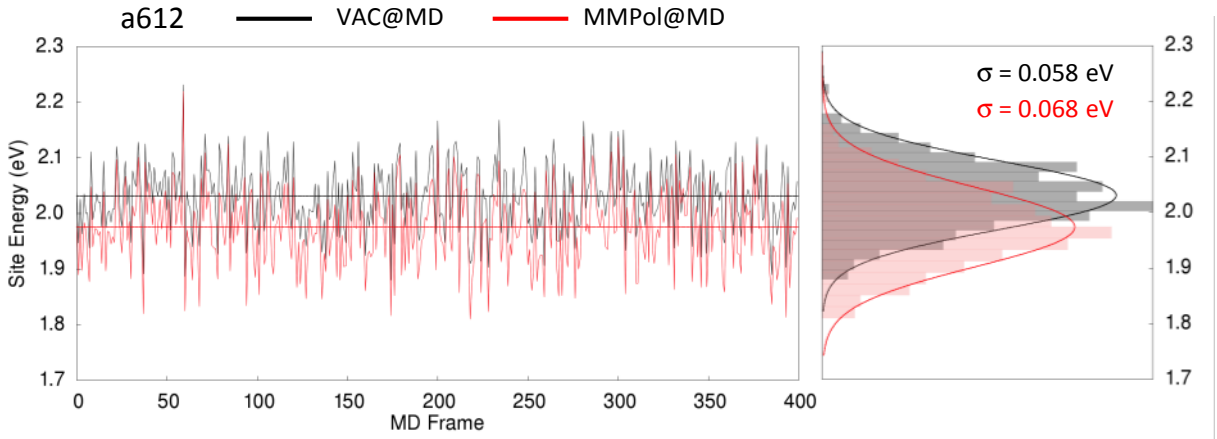

Figure S11. Site energies and relative distributions of pigment a612 along the MD trajectory computed in vacuum (black color) and with the MMPol description (red line).

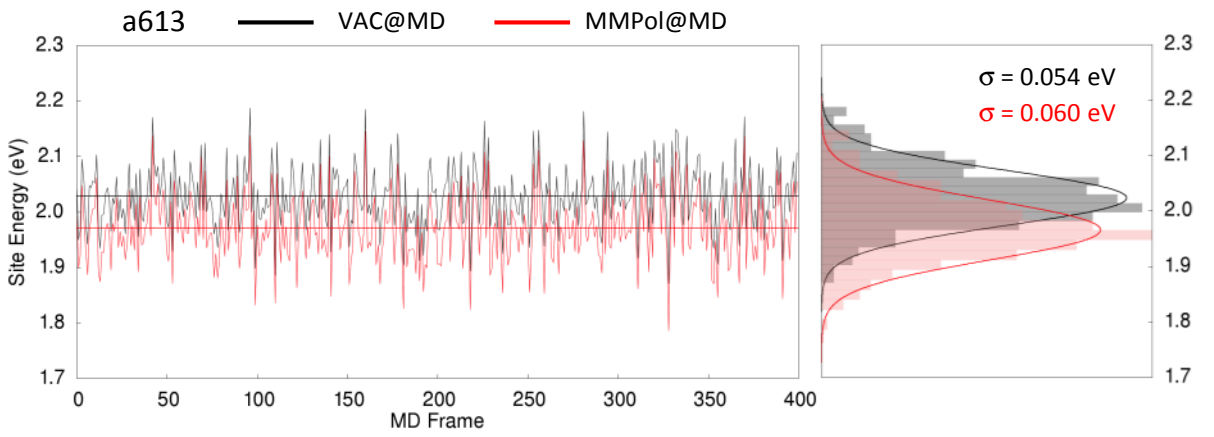

Figure S12. Site energies and relative distributions of pigment a613 along the MD trajectory computed in vacuum (black color) and with the MMPol description (red line).

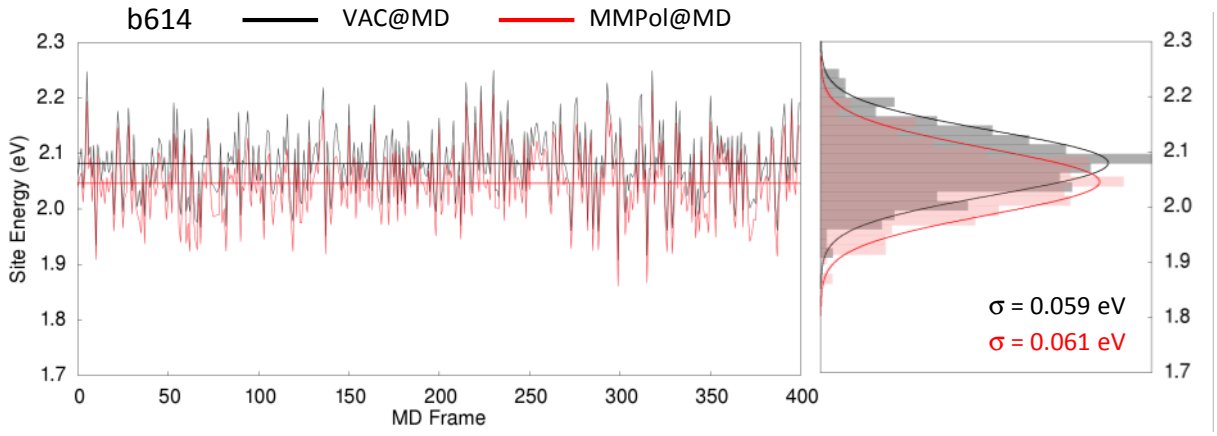

Figure S13. Site energies and relative distributions of pigment b614 along the MD trajectory computed in vacuum (black color) and with the MMPol description (red line).

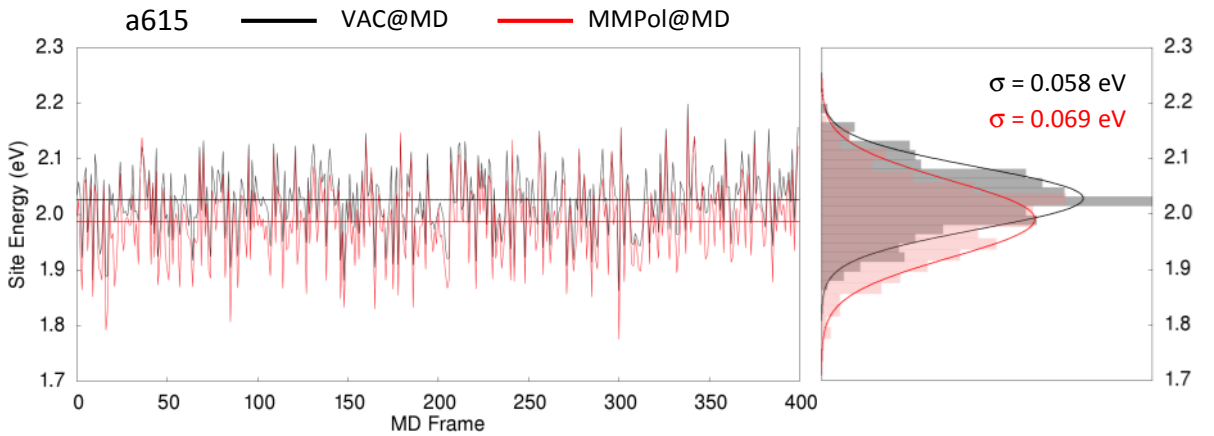

Figure S14. Site energies and relative distributions of pigment a615 along the MD trajectory computed in vacuum (black color) and with the MMPol description (red line).

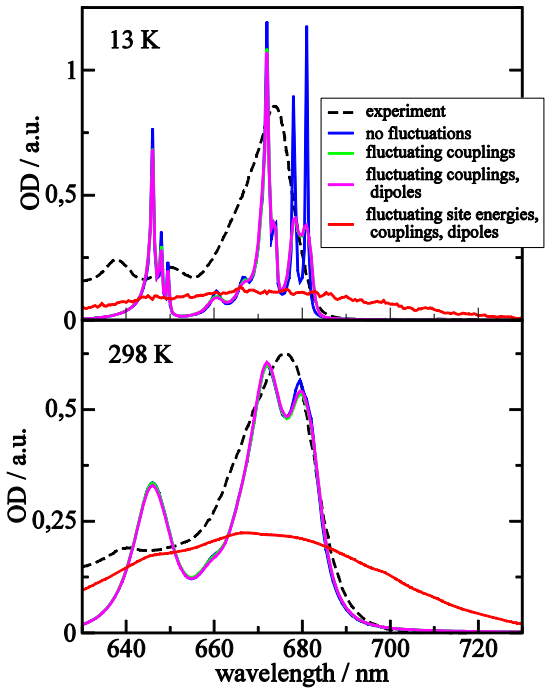

Figure S15. Linear absorption spectra simulated from the average excitonic description including fluctuation effects on couplings, dipoles, and site energies (colored lines) compared with the experiment (dotted black lines).

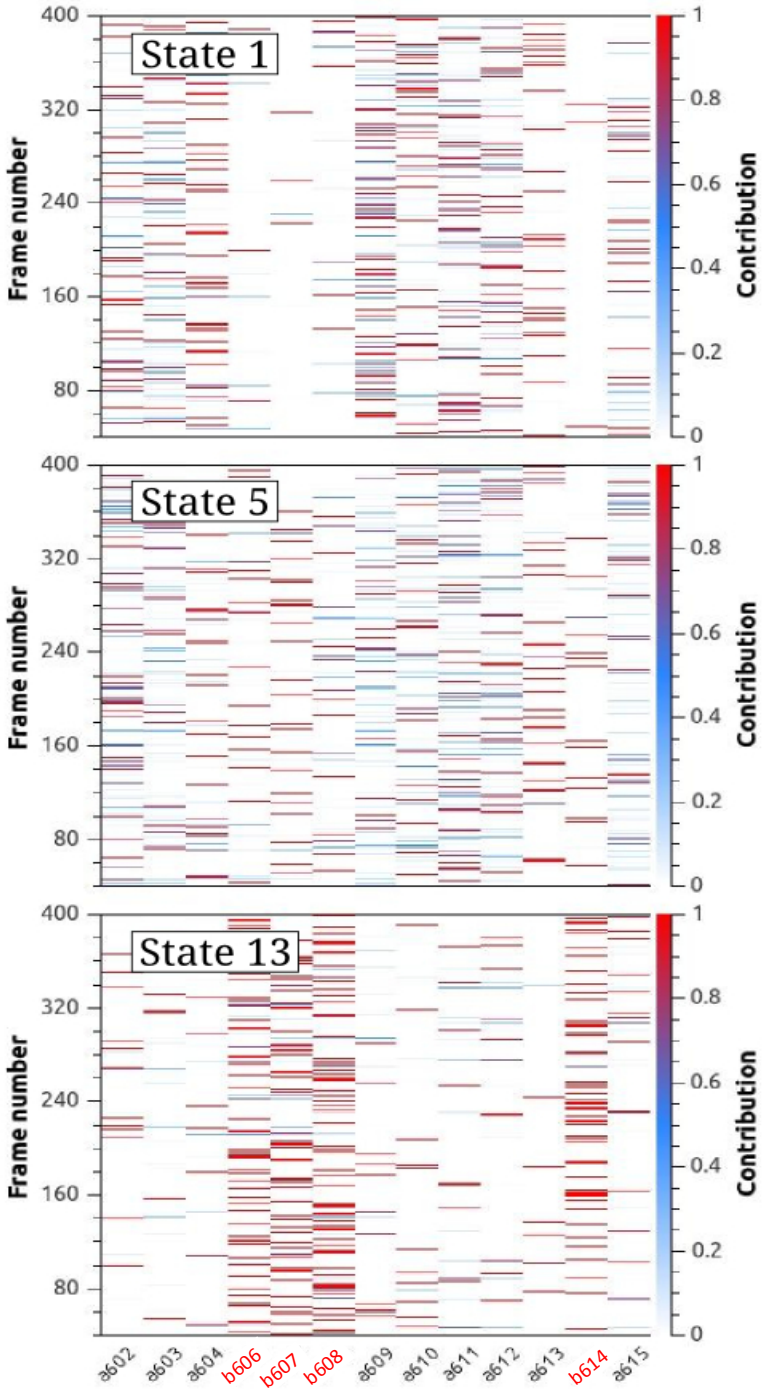

Figure S16: Evolution of the contribution ($|c_i^{(k)}|^2$) of each chromophore to the excitonic states 1 (top), 5 (middle), and 13 (bottom) along the MD trajectory.

3. Analysis of site energy shifts for pigments a604 and b608 in the crystal structure.

The MMPol@CRY calculations give the largest red-shift with respect to the range of variation of the other pigments for Chl a604 and Chl b608.

The two closest residues of Chl a604, Wat307 and Ile136, play a role in the stabilization of the ground state by about -19.5 Kcal/mol and -8.6 Kcal/mol respectively (see Figure S1a). However, their impact on the Q_y excited state is different. The excited state calculation performed by "switching-off" charge and polarizabilities of these residues indicates that Wat307 has no influence on the excitation, whereas Ile136 induces a red-shift of 0.02 eV. This suggests that small axial ligands, such as a water molecule, do not significantly affect the transition which does not involve the central Mg atom. On the other hand the H-bond between N-H of the ILE136 and C=O of a604 conjugated with the ring has a large influence on the transition. This finding is confirmed by an "enlarged" PCM calculation where the two residues Wat307 and Ile136 are included in the QM subsystem together with the pigment. In this case we obtain a site energy of 1.947 eV, i.e. 0.03 eV below the one calculated for the pigment only, and close to the MMPol site energy of 1.932 eV.

Also Chl b608 shows a similar local environment with respect to the a604 having a water molecule (Wat247) as axial ligand. If Wat247 is removed from the MMPol environment no changes in the site energy are observed. In this case, the interaction between the Chl C=O and the Arg101 N-H is smaller than in a604 because of the longer distance between O—H and we do not observe any significant shift in energy when Arg101 is removed. Thus, the large red-shift observed for Chl b608 can be ascribed to a global environmental effect and not to some specific residues.

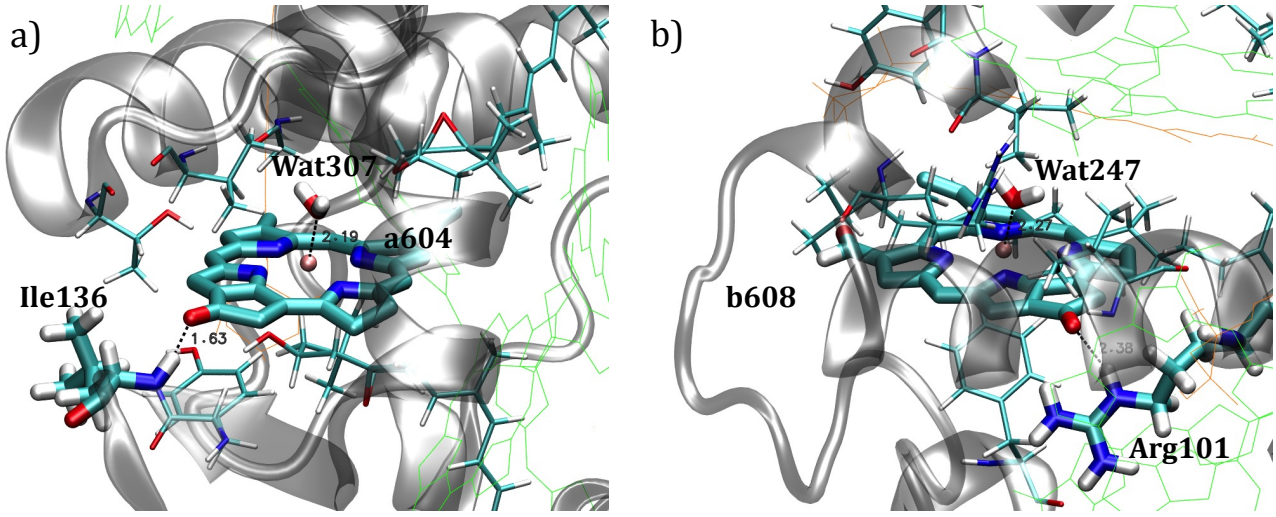

Figure S1. Local environment surrounding pigments a604 (a) and b608 (b) in the crystal structure. Closer residues are shown with tube representation.

References

1. I. Renge and K. Mauring, *Spectrochim. Acta. A. Mol. Biomol. Spectrosc.*, 2013, **102**, 301–13.

2. R. S. Knox and B. Q. Spring, *Photochem. Photobiol.*, 2003, **77**, 497.

3. G. Cinque, R. Croce, and R. Bassi, *Photosynth. Res.*, 2000, **64**, 233–42.